2004 ASME International Mechanical Engineering Congress and Exposition
November 13-20, 2004, Anaheim, California USA

IMECE2004-59928

NUCLEATE BOILING INSIDE THE EVAPORATOR OF THE PLANAR LOOP HEAT PIPE

Junwoo Suh
Department of Mechanical, Industrial and Nuclear Engineering
391 Engineering Research Center
University of Cincinnati, OH 45221
Phone: (513) 556-7447
suhj@email.uc.edu

Ahmed Shuja
Department of Electrical and Computer Engineering and Computer Science
372 Engineering Research Center
University of CincinnatiCincinnati, OH 45221-0030
Phone: (513) 556-4795
ashuja@ececs.uc.edu

Frank M. Gerner
Department of Mechanical, Industrial and Nuclear Engineering
598 Rhodes Hall
University of Cincinnati
Cincinnati, OH 45221-0072
Phone: (513) 556-2646

H. Thurman Henderson
Department of Electrical and Computer Engineering and Computer Science
390 Engineering Research Center
University of Cincinnati
Cincinnati, OH 45221-0030

ABSTRACT

The Loop Heat Pipe (LHP) under development is a next generation micro heat transfer device that utilizes the latent heat of a working fluid and has excellent transfer capacity compared with that of standard metallic cooling devices. A typical LHP consists of an evaporator, a reservoir (also called the compensation chamber), vapor and liquid lines, a subcooler, and a condenser. As heat is applied to the evaporator, all of the input energy goes into the evaporation of the liquid in the pores of the primary CPS wick or leak to the bottom. The nucleate boiling, which occurs beneath the primary wick in the evaporator, is a very significant phenomena. It affects critical operating issues, such as dry out of the primary wick. Using a clear evaporator machined from Pyrex glass, the nucleation, which occurred in the evaporator, was studied. De-ionized water was utilized as the working fluid.

INTRODUCTION

The loop heat pipe (LHP) is a thermal control and heat transport device. LHPs were originally invented and developed in the former Soviet Union in the mid 1980's, and has been employed in a reliable and versatile thermal control system for space applications. LHPs can transport very large thermal power loads over long distances through flexible, small diameter tubes and against high gravitational heads due to capillary forces in the evaporator. LHPs are two-phase heat transfer devices that utilize the latent heat and are completely self-circulating systems that have no mechanical moving parts and add no unwanted vibration to the spacecraft.

The Planar LHP at the University of Cincinnati

The traditional loop heat pipe was proposed by Maidanik et al. [1] in 1985. The conventional LHP consists of an evaporator, a reservoir (also called the compensation chamber), vapor and liquid lines, a subcooler, and a condenser. This evaporator consists of a cylindrical metallic case with an amorphous porous wick inserted into it.

A family of planar loop heat pipes is being developed at the University of Cincinnati. The work being conducted is based upon the use of a radically different type of wick structure made of planar coherent porous silicon (CPS). Using this technology, it is possible to achieve arrays of densely stacked micrometer sized capillaries or pores, which are essentially identical in diameter, in the common semiconductor material, silicon. This is in contrast to conventional amorphous porous ceramic wicks, which have pores of various diameters. In these wicks the largest pore dictates the value of the burst-through pressure and compromises the upper power level achievable by the loop heat pipe. Coherent porous silicon technology avoids such compromises through its uniformity. The resulting configuration is planar, which is more convenient for surface cooling applications for electronics, such as space solar power cells, and other flat or gently curved surfaces [2].

A schematic of the planar loop heat pipe, which is being developed at the University of Cincinnati, is shown in Figure 1. The device consists of an evaporator, condenser, and separate liquid and vapor lines. The compensation chamber is thermally and hydro-dynamically connected to the evaporator. Inside the evaporator of the planar loop heat pipe, there is a coherent

porous silicon wick structure, which maintains the separation between the liquid and vapor phases. In addition to the primary wick inside the evaporator, a secondary wick is situated between the compensation chamber and evaporator. It ensures that liquid remains available to the wick at all times.

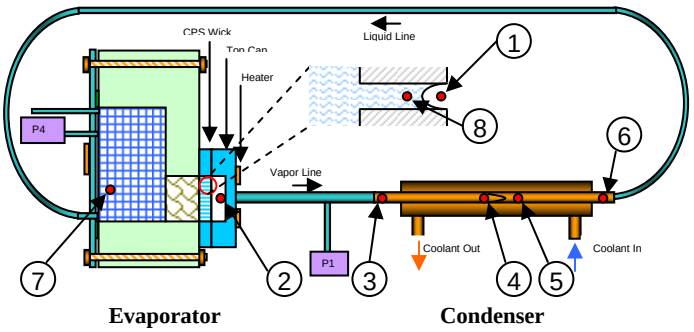

Figure 1. Schematic of the planar loop heat pipe

The very novel CPS technology was utilized in the fabrication of the porous wick in the loop heat pipe. Figure 2 (a) is a SEM micrograph of a sample of coherent porous silicon before through-holes have been produced. The CPS wick consists of an array of coherent pores produced by the photo-electrochemical dissolution of silicon in an aqueous solution of hydrofluoric acid. Its pores have an approximate diameter of 5 micrometers and the pitch, or center-to-center spacing, is 20 micrometers. During post processing, an aqueous solution of potassium hydroxide is used to etch the wafer backside of the sample to open the pores and produce the wick. The porosity pictured is 6.25 percent [3, 4].

The CPS wick was made from a two-inch n-type (100) silicon wafer and was bonded to the top layer (Figure 2 (b)). A nickel heater was integrated onto the backside of the silicon wafer to apply the uniform heat. The superheated vapor in the chamber of top cap exits through the hole to which the vapor line is soldered.

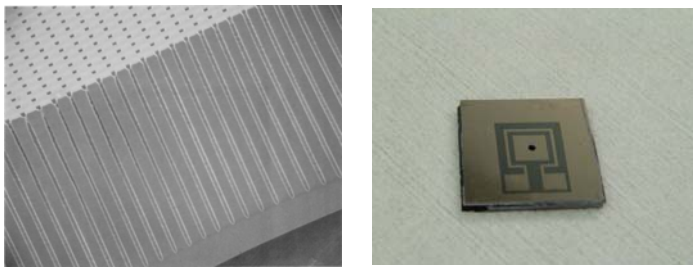

(a) Coherent porous silicon wick (b) Top cap

Figure 2. CPS wick and top cap

Thermodynamics of the planar Loop Heat Pipe

The operating principle of the planar LHP is summarized as follows. As heat is applied to the evaporator, liquid is vaporized. Menisci, which are formed at the liquid-vapor interface in the evaporator wick, are supported by capillary forces even though pressure forces push them down. Vapor condenses in the condenser and the capillary forces continue to push liquid back to the evaporator.The applied heat from the heat source provides the driving force for the circulation of the working fluid and no external pumping power is required.

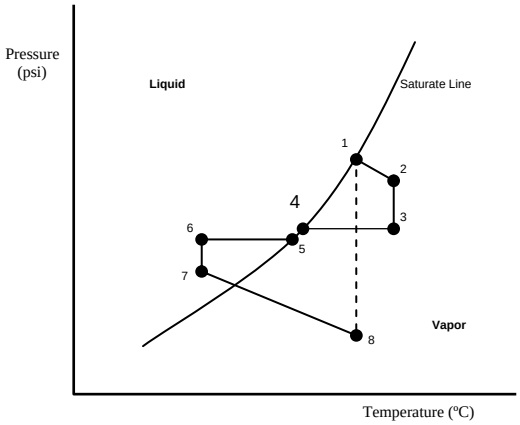

(a) Pressure-Temperature diagram

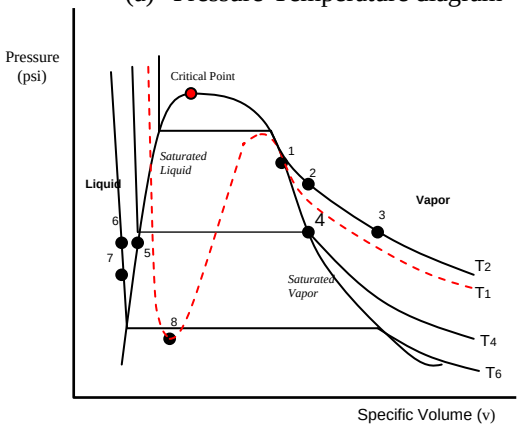

(b) Pressure-Specific volume diagram

Figure 3. The P-T and P-v diagram (not to scale)

Figure 3 (a) and (b) show the thermodynamic states of the working fluid at each of the physical locations shown in Figure 1. At point 1, just above the liquid-vapor interface in the pores of primary wick, the fluid is vaporized at the saturation temperature T_1 and pressure P_1. As the vapor flows through the vapor accumulation area, it becomes superheated at the exit of the evaporator (point 2) due to heating and a pressure drop. Assuming the vapor transport line to be perfectly insulated, the temperature of the vapor will remain unchanged. Because the pressure continues to drop along the vapor line, the vapor becomes more and more superheated, relative to the local saturation pressure, until it reaches the entrance of the condenser (point 3). The vapor loses its sensible heat and begins to condense inside the condenser (point 4). Between points 4 and 5, the pressure drops through the condenser tube and the saturated vapor condenses to saturated liquid. At point 5, vapor condensation is completed. The liquid continues to be subcooled until it exits the condenser at point 6. Because the liquid transport line is well insulated, the process between points 6 and 7 is an adiabatic process with a pressure drop. The subcooled liquid enters the compensation chamber at point 7. The heat leak from the primary wick heats the subcooled liquid in the compensation chamber. At point 8, the temperature of liquid equals that of saturated vapor (point 1). Even though point 8 is indicated in the vapor region in Figure 3 (a) the liquid in the pores of the primary wick is superheated liquid. Due to the input power, this superheated liquid evaporates to saturate

vapor in a constant temperature processes with the pressure change across the meniscus [5, 6].

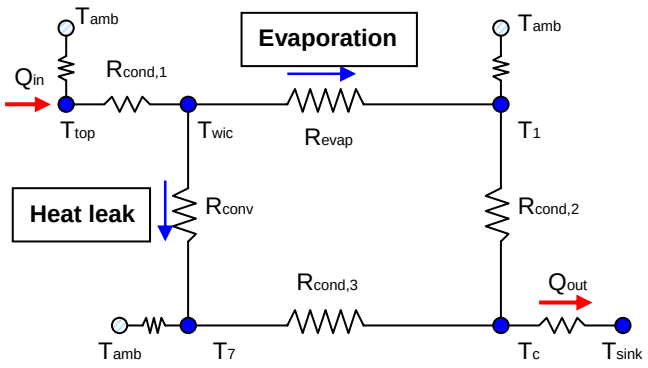

Figure 4. Thermal resistance network

Figure 4 shows the thermal resistance network of the planar loop heat pipe. The input power (Q_{in}) applied to the top plate is conducted to the primary wick. By neglecting the heat loss to the ambient, all of the input energy goes into the evaporation of the liquid in the pores of the primary CPS wick or leak to the bottom.

$$\dot{Q}_{in} = \dot{Q}_{evapration} + \dot{Q}_{heat\cdot leak} = \dot{m} h_{fg} + hA(T_{wick} - T_7) \tag{1}$$

If nucleate boiling occurs on the bottom side of the coherent porous silicon wick, it could lead to wick "depriming" and cause equipment failure. It is necessary to monitor any nucleate boiling, which occurs inside the evaporator of the micro loop heat pipe.

Nucleation Limit

There are several operating limits in the planar loop heat pipe; such as, the capillary, sonic, superheated liquid and nucleate boiling limits. The nucleation limit, specifically, is considered here. Nucleate boiling, by definition, is characterized by the preferential formation of vapor bubbles at certain locations known as "nucleation sites". This occurs when the liquid temperature is increased to a temperature above the saturation temperature in contact with a surface [7]. The classical equation for the nucleate boiling is:

$$r_c = \frac{2\sigma T_{Sat}}{\rho_v h_{fg} (T_{Wall} - T_{Sat})} \tag{2}$$

The minimum cavity mouth radius for nucleation to occur at a nucleation site is given by r_c. The onset of nucleate boiling can be predicted if the relation between the surface roughness, the pressure of the evaporator chamber, and the temperature of the surface is established.

When the input power is applied through the top cap, the heat is conducted to the primary wick. The temperature difference between the upper and bottom side of CPS wick is not much due to the high thermal conductivity of the silicon. The pressure in the upper chamber (P_1) is higher than the pressure in the compensation chamber (P_7) (Figure 5 (a)). As with shown in Figure 5 (b), T_A is the saturation temperature corresponding to the upper chamber (P_1).

$$T_A = T_{Sat}(P_1) \tag{3}$$

The temperature, T_B, is the corresponding value of pressure in compensation chamber (P_7) on the saturation curve.

$$T_B = T_{Sat}(P_7) \tag{4}$$

The wall temperature (T_{wall}) to cause the nucleate boiling can be acquired from the Equation (2).

$$T_C = T_{wall} = \left(1 + \frac{2\sigma}{\rho_v h_{fg} r_c}\right) T_{Sat}(P_7) \tag{5}$$

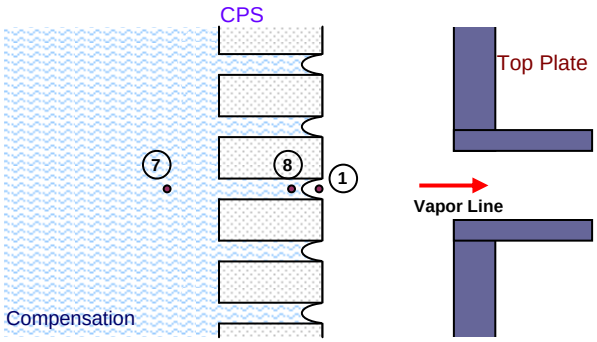

(a) Steady state condition in the evaporator

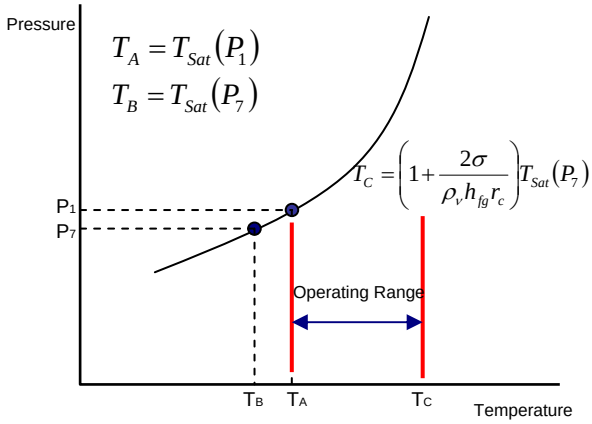

(b) Pressure-temperature curve

Figure 5. System operation region

Like Figure 5 (b), the system operating range can be predicted. When the primary wall temperature (T_{wall}) is less than T_A there is no evaporation in the pores of CPS wick. Because the temperature does not reach the saturation temperature the liquid remains in the subcooled condition. If the wall temperature is passed through the temperature, T_C, then it is easier to initiate the nucleate boiling from the bottom side. Once the nucleate boiling is occurred bellowed the primary wick it is undesirable for the proper operation in two aspects. First, majority of input energy go for the heat leak to the compensation chamber. This can be shut down the pumping mode which pushes the liquid in the evaporator to the

condenser. Second, the vapor layer, which would form below the CPS wick, would also block fluid flow through the loop.

Hamdan et al. [8] proposed the steady state LHP model which was described by conservation equations, thermodynamic relations, capillary and nucleate boiling limits. The seven major independent equations consisted of seven unknown independent variables, T_1, T_8, T_7, $\dot{m}$, β, $\rho_{v,h}$, $\rho_{v,cc}$, and were solved using a simple iteration technique which took into account the proper boundary conditions. The maximum superheated temperature (ΔT_t) in the liquid was:

$$\Delta T_t = \left(\frac{v_{fg,c}T_c}{h_{fg,c}}\right)\left[\frac{8\mu_{l,c}\dot{m}(l-l_v)}{\pi\rho_{l,c}R^4} + \frac{8\mu_{v,c}\dot{m}l_v}{\pi\left(\frac{\rho_{v,c}+\rho_{l,c}}{2}\right)R^4} + \frac{8\mu_{l,c}\dot{m}L}{A\varepsilon\rho_{l,c}r^2}\right] \quad (6)$$

and should be less than the nucleate boiling limit (ΔT_{max}) for the proper operation of the whole system.

$$\Delta T_t \le \Delta T_{\max} \approx \frac{2\sigma T_{sat}}{\rho_v h_{fg} R_f} \quad (7)$$

A nucleate boiling limit was also suggested by Hamdan et al [9]. The nucleate boiling limit (ΔT_{max}) was calculated by using the pore radius. This limit was compared with the maximum superheated temperature (ΔT_t) solved by the mathematical model. In this way, the maximum heat load could be predicted.

It should be noted that Hamdan et al.'s nucleation limit occurred at the bottom of the primary wick. It is possible that the operate range shown in Figure 5 (b) is very small. If so, others have suggested that it is possible to prevent the nucleate boiling by controlling the effective pore size of the secondary wick. The theory being that if the effective pore size is small enough and the thickness of the secondary wick is large enough, the nucleate boiling will not occurred in the secondary wick and the temperature at the bottom of the secondary wick will be behind the nucleate boiling temperature. This issue will be explained in future study.

EXPERIMENTAL SETUP AND PROCEDURE

To understand the nucleation, which occurred below the primary wick in the evaporator, the transparent evaporator section was constructed. This planar loop heat pipe is being developed for future space applications as a thermal control device, so the vertical and horizontal direction tests were conducted to understand the effects of orientation.

See-Through Evaporator

The evaporator is an essential part of entire closed loop system. The phenomena occurring in it must be well understood for proper operation. To monitor and study nucleation in the evaporator, a clear evaporator, which consisted of a top plate and a compensation chamber, was constructed from Pyrex glass.

The top cap consisted of three layers. The top layer was a nickel heater integrated onto one side of a silicon wafer to provide the uniform application of heat to the primary coherent porous silicon wick through the middle frame layer. The middle silicon layer was a one square centimeter area etched into a 1.7 by 1.7 square-centimeter piece of silicon. The etched area functioned as the vapor collection chamber (Figure 6 (a)). The bottom layer was a primary coherent porous silicon wick. To protect against leakage, these three plates were bonded together with VACSEAL and baked in an oven for one hour at 260 ºC. As is shown in Figure 6 (b), the top cap was connected by solder to a stainless steel tube to which the vapor transport line was attached. The stainless steel tube was four centimeters in length, and had an inner diameter of one millimeter and an outer diameter of 1.5 millimeters. The top cap was positioned in the evaporator section, which consisted of a Pyrex 7740 glass compensation chamber and a Pyrex glass back plate. The split-level compensation chamber consisted of two cylindrical volumes, each of which had its own diameter. A diamond drill was used to produce the two different sized volumes. The diameters and lengths of the smaller and larger volumes, respectively, were 1.0 centimeter and 0.6 centimeters and 2.54 centimeters and 0.9 centimeters. The glass back plate enabled visual observation of the activity below the CPS wick during the tests. High-Temp RTV SILICONE was chosen as the sealant to bond together the top cap and evaporator section because it made it possible to separate the top cap from the evaporator section without damage to the Pyrex glass surface.

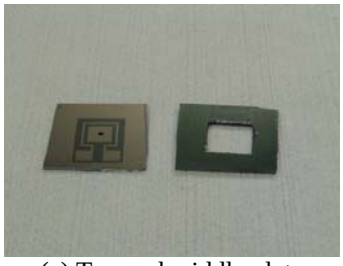

(a) Top and middle plate

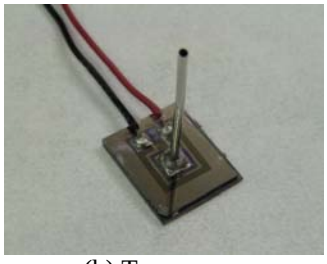

(b) Top cap

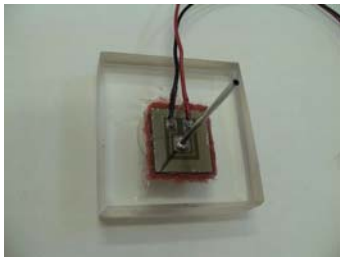

(c) Top cap and evaporator

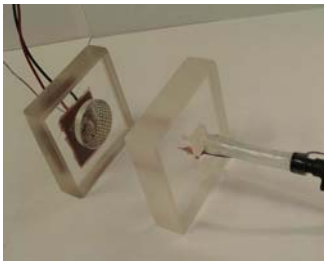

(d) Transparent evaporator

FIGURE 6. The top cap and compensation chamber.

The transparent Pyrex glass back plate was designed to seal the compensation chamber in the evaporator section and to enable observation of the phenomena, which occurred below the CPS wick. Three holes were machined into the back plate with a diamond drill. One hole was the input for the pressure sensor. A thermocouple to the compensation chamber was placed through the second hole, which was then sealed with silicone. The working fluid was supplied through the third hole, which was linked to the transparent liquid line after filling. Figure 7 shows the inside sections of the transparent evaporator. The stainless steel retaining mesh was used in the compensation chamber only when the secondary wick, quartz

wool, was utilized in the evaporator to secure it in place below the primary CPS wick. The evaporator section and back glass plate were also sealed with Silicone RTV.

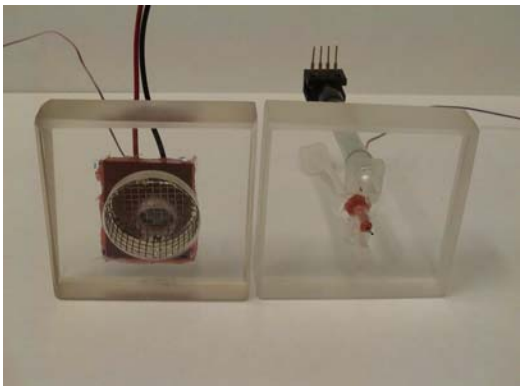

FIGURE 7. Inside surface of the evaporator

Vertical Orientation

Figure 8 shows a nucleation test conducted with the see-through evaporator. Type T thermocouples were used to measure the temperature of the top cap and liquid in the compensation chamber. A pressure sensor was connected to the compensation chamber to measure pressure at the bottom side of the primary CPS wick. The insulation was only placed on the top cap side to insulate against heat leakage to the ambient.

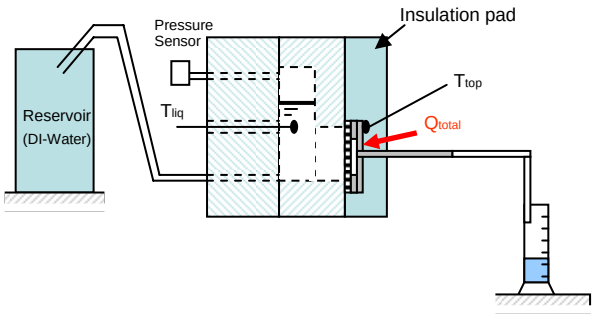

(a) Schematic of experiment setup (vertical direction)

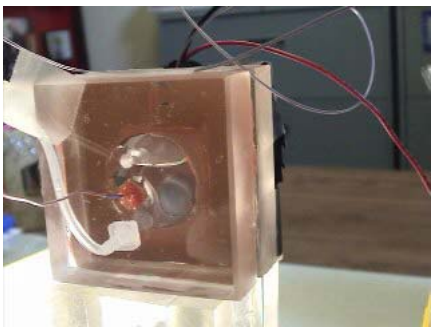

(b) View from the compensation chamber side

Figure 8. Schematic and photograph of the experiment

Before heat was applied to the evaporator, 3.5 milliliters of de-ionized water, the working fluid, were injected into the compensation chamber with a syringe. No de-gassing procedure was performed. The total volume of the compensation chamber was 4.6 milliliters. After the compensation chamber had been filled with the working fluid, the liquid transport line, a transparent silicone tube, was connected to the reservoir by a plastic connector (Figure. 8 (b)). Due to the capillary force of the primary CPS wick there was no liquid flow to the vapor line. The input power was calculated from the power supply voltage and current settings. A camcorder was used to film the activity observed at the bottom of the CPS wick. After the system reached a steady state condition, liquid which condensed from vapor in the vapor line was collected in a graduated cylinder.

Horizontal Orientation

In the horizontal orientation test, the condition was almost the same as in the vertical orientation with the exception of the direction of gravity. The visualized evaporator was rotated 90 degrees counter clockwise; the CPS wick faced downward. A specific filling procedure was used to supply the working fluid into the compensation chamber. The evaporator sat on a jig designed to hold it with the back Pyrex glass on top of the evaporator section. De-ionized water was injected by a syringe through the inlet hole that was connected to the liquid transparent line. The liquid was filled from the bottom side due to the gravity force. Even though there were micrometer sized pores in the CPS wick there was no burst through due to the capillary force of CPS wick. The reservoir and compensation chamber were connected to the transparent silicon tube. The evaporator was rotated 180 degrees after the compensation chamber was completely filled with the working fluid. Any air that remained in the compensation chamber was removed using a syringe connected to the vapor line. Unfortunately, there was no way to determine whether or not there was any air remaining inside the top cap. Tests similar to those conducted in the vertical orientation were then performed.

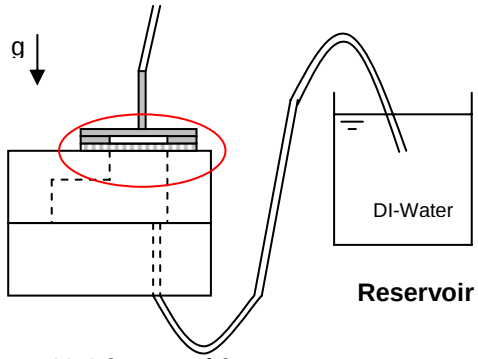

(a) Schematic of the experiment setup

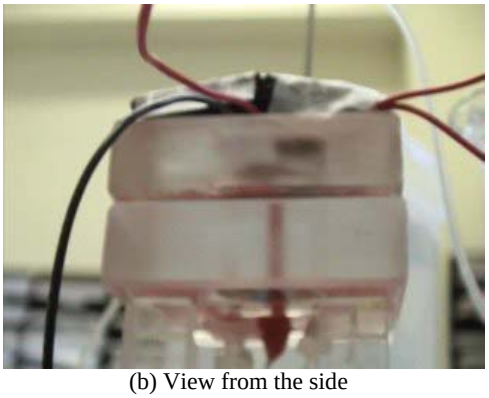

(b) View from the side

FIGURE 9. Schematic and photograph of the experiment

RESULTS AND DISCUSSION

Figure 10 was the top side roughness of the coherent porous silicon (CPS) wick measured by the surface profiler. The roughness was characterized in terms of the RMS roughness (R_a) using a KLA Tencor P-10 Profiler. This CPS wick was etched 50 μm between the etch pitch and a diameter as a 10 μm. Profiler sets as 500 μm of the total scanning length, 50 μm/s of the scan speed and 50 Hz of the sampling rate.

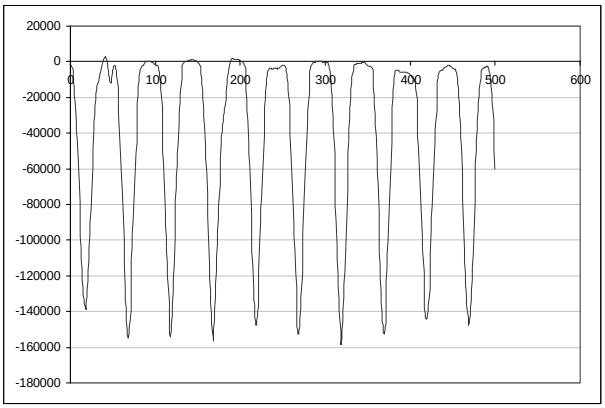

Figure 10. Top side roughness of the CPS wick

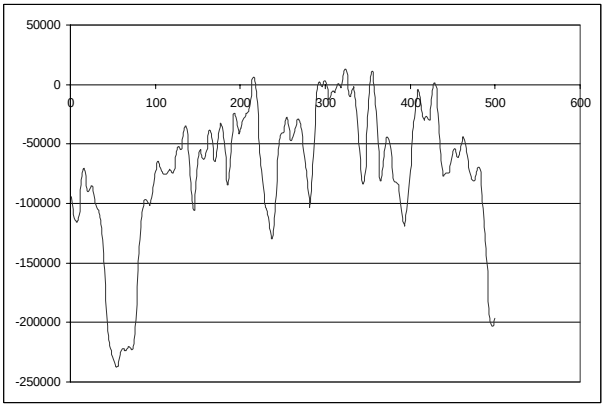

Figure 11. Bottom side roughness of the CPS wick

In case of the top side, there were 10 pores within the 500 μm length and pore depth was look like a cone due to the limitation of the measuring tip. The y-coordinate was the depth of the surface and its dimension was angstrom (Å) in Figure 10 and 11. RMS roughness of top side was 3.1037 μm and the bottom side was 4.981 μm. Actually it was needed to clarify which was the best indicator of cavity size. The bottom side of the roughness was rougher than top side and the shape of pattern was irregular (Fig.11). The differences in the typography between the top and bottom portion of the wick structure was due to the post processing in KOH solution. The silicon pore structure was first formed with the CPS etching technique (photon pumped electrochemical etching). In this step the pres were not etched all the way through so the substrate must be etched back to reach the pore front. During the process the aggressive nature of the etchant caused the roughing of the surface.

From the previous results of RMS roughness, the nucleation boiling limit was calculated. Hamdan et al. [9] predicted that as heat load through the top increase, the temperature of the top chamber (T_1) and the below temperature of the liquid-gas interface (T_8) increased when the phase change temperature (T_c) inside the condenser was fixed as 80 ºC. Using the maximum superheated temperature (ΔT_t) in the liquid the nucleation limit was suggested around 370 W/cm^2 shown in Figure 12. In this prediction, the pore radius was used instead of the actual R_a (average RMS roughness) value of the liquid side of the CPS wick.

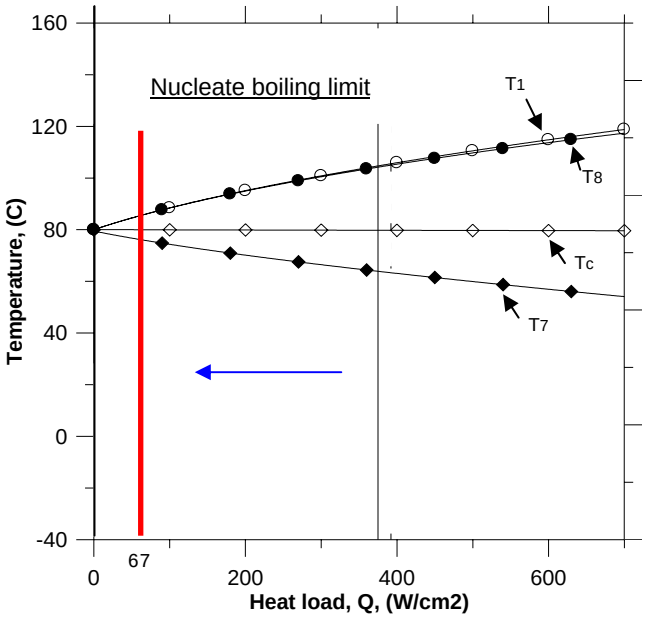

Figure 12. Nucleation boiling limit (T_c =80 ºC)

But the exact value of nucleate boiling limit which was calculated by the measured RMS roughness was a quite difference. Like an equation (7), it was required several values to acquire this limit. Surface tension, latent heat, and density of the vapor were obtained from the properties table. The maximum heat load was calculated as 67 W/cm^2 based on the suggested data (T_1 and T_7) and this was much lower than the previous prediction.

"Pumping" Mode in the Evaporator

In the first vertical orientation test, a primary CPS with a capillary pressure of 3.444 pounds per square inch was utilized without the secondary wick in the compensation chamber. The average pore radius was assumed to be 5.437 micrometers. The initial temperature of entire system was 23.5 ºC and gradually increased as 9.39 Watts was applied to the top plate heater. Vapor bubbles formed on the CPS wick surface at quite a low temperature compared to the saturation temperature because it was not under vacuum and air was still dissolved in the de-ionized water (Figure 13 (a)). As the temperature of the CPS wick increased, the volumes of the vapor bubbles also increased. Shown in Figure 13 (b), the formed vapor bubbles rose and merged together at the top area on the wick due to buoyancy. The large bubble, which formed at the top area of the CPS wick, rose to the liquid-air interface and the tiny bubbles formed again. These vapor bubbles increased and

decreased in volume as if they were breathing. Other groups have also observed this "breathing wick" phenomenon [10]. As liquid condensed in the vapor line, it fluctuated back and forth (Figure 13 (c)). It was assumed that the liquid evaporated in the pores of the primary CPS wick and then condensed in the stainless steel tube due to its low temperature. The system reached and remained in a steady state condition for one and half hours. The big vapor bubble remained at the top site continuously increased its volume and rose up. Many of the small vapor bubbles reformed on the surface of CPS wick. They were "breathing in and out" in synchronization with the fluctuating condensed liquid. The top plate temperature was 101.3 ºC and the liquid temperature in the compensation chamber was 80.5 ºC. The amount of condensed liquid, which poured down from the vapor line into the graduated cylinder, was measured as 7.6 milliliters for twenty-five minutes. Assuming that all of the collected liquid was due to evaporation, the corresponding evaporation energy was calculated to be 11.436 Watts. From this result, it was speculated that there was some unknown mechanism, which pushed the liquid to the vapor line, because the output energy calculated from the collected liquid exceeded the input energy.

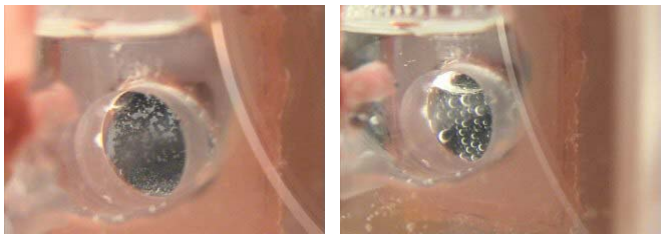

(a) Vapor bubbles onset (b) breathing vapor on the CPS wick

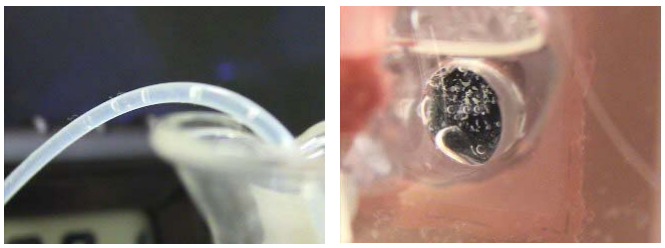

(c) Fluctuating liquid (d) Nucleate boiling

FIGURE 13. "Pumping" Mode in the evaporator

Several tests were conducted at various input powers. At the input powers of 6.86 Watts and 9.39 Watts, the activity below the CPS wick prior to reaching steady state was similar to the previous description. Some amount of liquid was collected from the vapor line even though the mechanism was not yet understood. No liquid was collected at low input powers such as 4.16 Watts. At the input power of 12.63 Watts there was a period during which liquid was collected. When the temperature of the top plate suddenly increased to approximately 134 ºC the collection of liquid stopped. Unlike in the previous test, nucleate boiling was observed on the CPS wick and the liquid in the vapor tube stopped fluctuating (Figure 13 (d)). One possible explanation for this phenomenon is that all of the energy went into the nucleate boiling.

Three Regions

Attempts to measure the temperature of the CPS wick were abandoned because the CPS wick is so easily damaged and pores in the wick were blocked if the thermocouple was attached to the surface with the epoxy. The temperature of top plate and the liquid in the evaporator were measured instead of the CPS wick. The measured value of the top plate temperature was suspicious; a little low due to the thick layer of epoxy between the surface and tip of thermocouple.

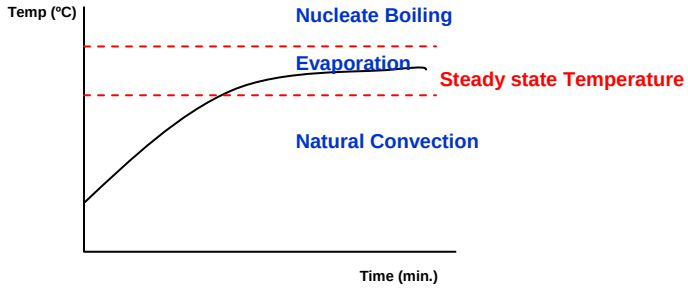

Figure 14. Nucleate boiling curve (Temp. vs. Pressure)

Table 1. Steady state temperature of top plate and liquid

Q	4.16 W	6.864 W	9.39 W	12.63 W
Ttop	92.3	94.3	101.3	133.9
Tliq	72.3	76.8	80.5	84.6
Pumping	×	O	O	O → ×

The time during which the CPS wick reached the steady state temperature depended on the input power. As shown in Figure 14, it was assumed that there were three regions: natural convection, evaporation, and nucleate boiling. If the steady state temperature was reached in the natural convection region, as in the test in which 4.16 Watts was applied, vapor bubbles formed only on the surface. If this temperature was reached in the evaporation region, the volumes of the vapor bubbles expanded and contracted. A "pumping" mode was observed. In the case of 12.63 Watts of input power, as the transient temperature of the wick passed the natural convection and evaporation regions, the vapor bubbles formed and their volumes oscillated. As the wick temperature passed the maximum temperature and reached the nucleate boiling region, nucleate boiling below the CPS wick was observed. Once the nucleate boiling occurred the liquid which had condensed in the tube stopped fluctuating. No liquid from the vapor line was collected. The majority of the input energy was wasted on nucleate boiling and not in evaporation.

Depriming of the Primary Wick

In the vertical orientation test, a primary wick partially deprimed during the operation. The continued pumping of a partially deprimed evaporator was previously reported by another group [10]. They explained that most large diameter evaporator CPL's continuously work above the transport limits predicted by theory. The theory assumes that the evaporator deprimes as soon as vapor bubbles penetrate the primary wick and bubbles form inside the liquid core.

In the horizontal orientation test, 4.15 Watts was applied to the top plate after the compensation chamber was fully filled

with de-ionized water. The formation of small bubbles below the wick was observed and slowly increased in size as the temperature increased (Figure 15 (a)). Unlike in the vertical orientation, the vapor bubbles merged together below the primary CPS wick and remained in their position but their volume increased. The vapor eventually covered the total area below the CPS wick. This depriming phenomenon is shown in Figures 15 (b) and (c).

The function of secondary wick was to keep the wick wet and collapse the vapor bubbles, which formed below the CPS wick. Quartz wool was used as a secondary wick to monitor its effect. The amount of 0.0087 grams was inserted into the smaller volume of the split-level compensation chamber. The stainless steel retaining mesh was used to push the secondary wick to the primary wick. Its porosity of the secondary wick was calculated to be 92 %. An input power of 7.13 Watts was applied to the evaporator. The steady state temperatures reached by the top plate and liquid were 114.7 °C and 62.6 °C, respectively. In this case, there was no liquid condensing from the vapor line even though there was pumping in the test at the same without the secondary wick. It was speculated that the vapor bubbles, which formed in the secondary wick due to their high radii, blocked the area below the primary wick. "Depriming" occurred and shut down the pumping operation in the evaporator (Figure 15 (d)).

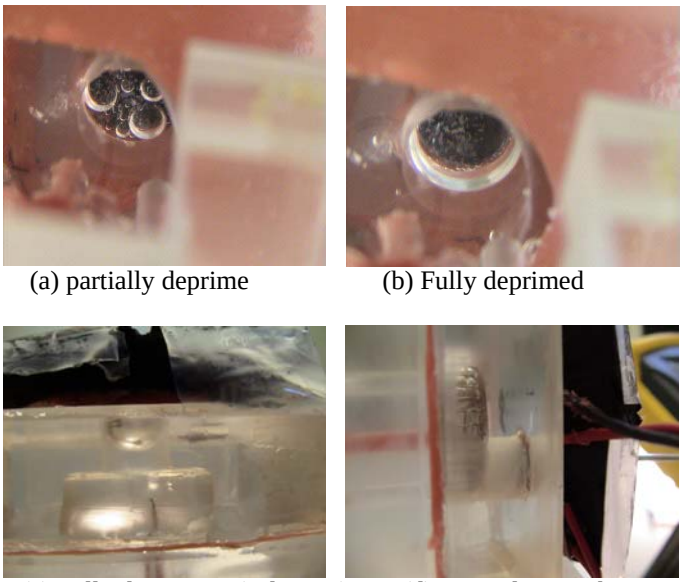

(a) partially deprime (b) Fully deprimed

(c) Fully depriming (sideview) (d) Secondary wick

FIGURE 15. Depriming of the device

CONCLUSIONS AND RECOMMENDATIONS

There was an operating range in which the liquid could be properly pumped from the compensation chamber to the vapor line. That range was depending on the temperature of primary wick. The pumping mechanism was not observed at low input powers. In the case of the high input power, all of the energy caused nucleate boiling on the backside of the primary wick. Pumping ceased when nucleate boiling was observed in the evaporator. The nucleate boiling is significant factor in determining the nucleation limit and depriming.

Primary wick depriming is related to the direction of gravity. In the case of vertical orientation, full depriming due to buoyancy was not observed and partial depriming did not cause the shut down of the pumping mechanism. In the horizontal orientation, after the onset of vapor bubbles formation below the primary CPS wick full depriming did not take a very long time.

It was assumed that the secondary wick would collapse any vapor bubbles that formed below the primary wick. That was not true in this test with the 92 % porosity quartz wool. Vapor bubbles formed in the secondary wick due to large radii and caused depriming of the primary wick. The density of the secondary wick should be considered a very important variable.

ACKNOWLEDGMENT

Major support for the project was received from the NASA John H. Glenn Research Center at Lewis Field (GRC) under various grants, NSF/NASA/EPRI Space Power Systems, the University of Cincinnati and the NASA Graduate Student Research Program. The authors wish to express their appreciation to the Advanced Power and On-Board Propulsion Division of NASA's Cross Enterprise Technology Development Program, especially Ken Mellott of GRC for their continued support of and input to the project, and for their many efforts on our behalf. The authers would like to appreciate Debra Cytrynowicz, Praveen Medis and Srinivas Parimi of University of Cincinnati for their support and valuable suggestion.

NOMENCLATURE

A : Wick cross sectional area, m^2
CPS : Coherent porous silicon
h : Heat transfer coefficient, $J/m^2 \cdot K$
h_{fg} : Latent heat of evaporation, J/kg
l : Tube length, m
L : Wick thickness, m
$\dot{m}$: Mass flow rate, kg/s
R : Tube radius, m
R_f : Surface roughness, m
T_S : Saturation temperature, K
T_W : Surface temperature, K

Greek symbols

ε : Porosity
β : Volumetric ratio, $V_{v,cc} / V_{cc}$
μ : Dynamic viscosity, $kg/s \cdot m$
ρ_v : Vapor density, kg/m^3
σ : Surface tension, N/m

Subscript

c : Condenser
cc : Compensation chamber
l : Liquid
v : Vapor

REFERENCES

[1] Maidanik, Y., Vershinin, S., Kholodov, V., and Dolggirev, J., 1985, "Heat Transfer Apparatus", US patent 4515209.

[2] Cytrynowicz, D., Medis, P., Parimi, S., Shuja, A., Henderson, H.T., and Gerner, F.M., "The MEMS Loop Heat Pipe Based on Coherent Porous Silicon – The Modified System Test Structure," in *proceedings of Space Technology and Applications International Forum (STAIF-2004)*, edited by M.

El-Genk, AIP Conference Proceedings 669, New York, 2004, pp. 164-173.
[3] Cytrynowicz, D., Hamdan, M., Medis, P., Shuja, A., Henderson, H.T., Gerner, F.M., and Golliher, E., "MEMS Loop Heat Pipe Based on Coherent Porous Silicon Technology," in *proceedings of Space Technology and Applications International Forum (STAIF-2002)*, edited by M. El-Genk, AIP Conference Proceedings 608, New York, 2002, pp. 220-232.
[4] Hölke, A., Pilchowski, J., Henderson, H. T., Saleh, A., Kazmierczak, M., Gerner, F. M., Baker, K., "Coherent Macroporous Silicon as a Wick Structure in an Integrated Micro-Fluidic Two - Phase Cooling System," *Proceedings of the SPIE Conference on Microfluidic Devices and Systems*, Santa Clara, California, September 21 - 22, 1998.
[5] Ku, J., "Operating characteristics of loop heat pipes," Society of Automotive Engineers, 1999-01-2007, 1999.
[6] Atabaki, N., and Baliga, B.R., "Steady-State Operation of a Loop Heat Pipe: Network Thermofluid Model and Results," *Proceeding of 2003 ASME International Mechanical Engineering Congress*, paper No. IMECE2003-43968, pp. 73-85, 2003.
[7] Kandlikar, S.G., Shoji, M., and Dhir, V.K., "Nucleat Boiling", Handbook of Phase Change: Boiling and Condensation, Editor Kandlikar S., Shoji M., and Dhir V., 1999, Ch. 4, pp 71-120.
[8] Hamdan, M., Cytrynowicz, D., Medis, P., Shuja, A., Gerner, F.M., and Henderson, H.T., 2002, "Loop Heat Pipe (LHP) Development by Utilizing Coherent Porous Silicone (CPS) Wicks," *ITHERM International Conference on Thermal Phenomena in Electronic Systems*, San Diego, California
[9] Hamdan, M., Gerner, F.M., and Henderson, H.T., 2003 "Steady state model of a loop heat pipe (LHP) with coherent porous silicon (CPS) wick in the evaporator", *19th Annual IEEE Semiconductor Thermal Measurement and Management Symposium (SEMI-THERM)*.
[10] Ku., J., Swanson, T.D., Herold, K., and Kolos, K., "Flow Visualization within a Capillary Evaporator," *SAE international*, Warrendale, PA, SAE paper No. 932236: pp. 1424-1432, 1993.
[11] Cytrynowicz, D., Hamdan, M., Medis, P., Henderson, H.T., Gerner, F.M., and Golliher, E., "Test Cell for a Novel Planar MEMS Loop Heat Pipe Based on Coherent Porous Silicon," in *proceedings of Space Technology and Applications International Forum (STAIF-2003)*, edited by M. El-Genk, AIP Conference Proceedings 654, New York, 2003, pp. 227-238.